Volume 9
Number 4
April 2024
Pages 497–658

Nanoscale Horizons

The home for rapid reports of exceptional significance in nanoscience and nanotechnology

rsc.li/nanoscale-horizons

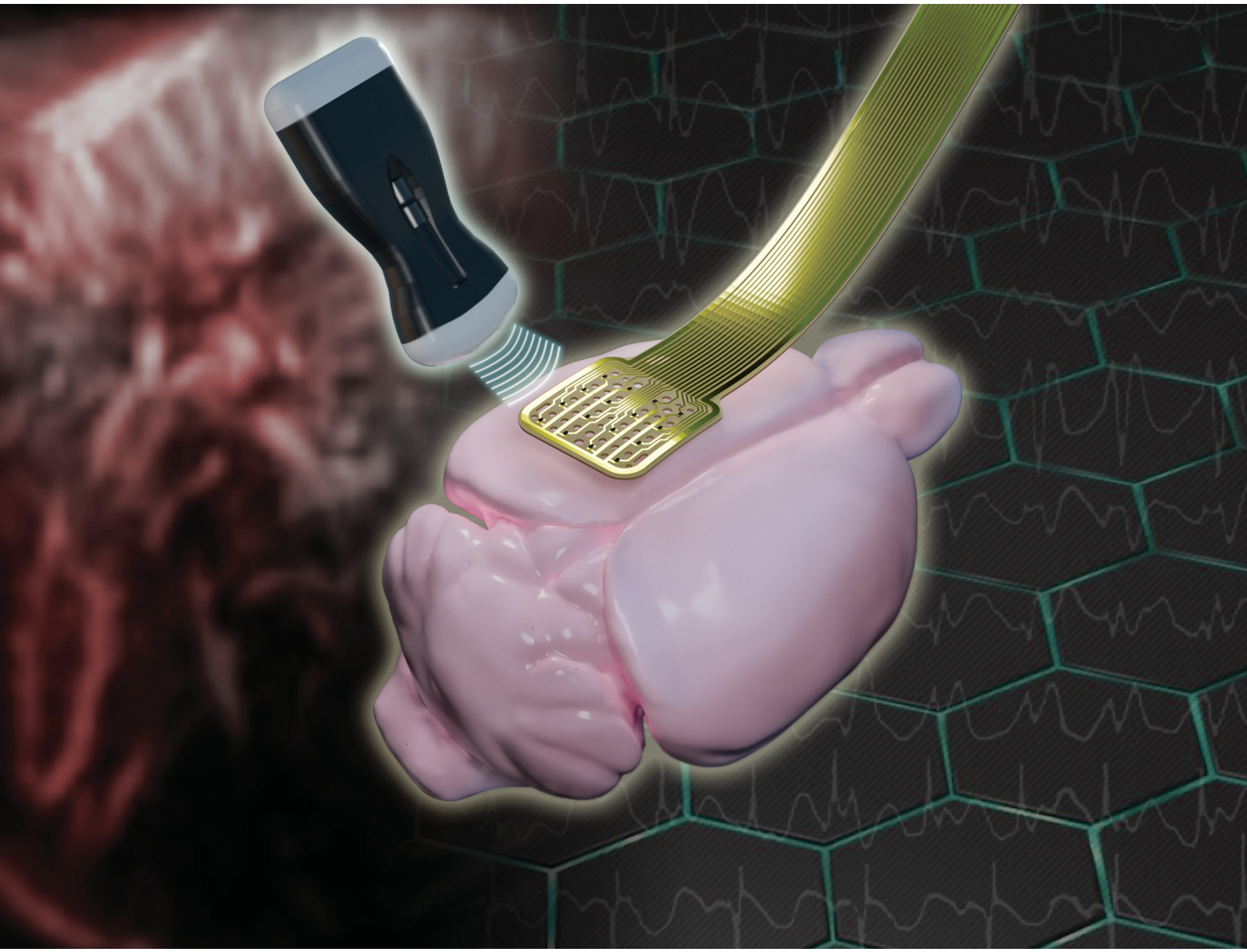

ISSN 2055-6756

COMMUNICATION

Anton Guimerà-Brunet, Rob C. Wykes *et al.*
Concurrent functional ultrasound imaging with graphene-based DC-coupled electrophysiology as a platform to study slow brain signals and cerebral blood flow under control and pathophysiological brain states

ROYAL SOCIETY OF CHEMISTRY

NCNST

Nanoscale Horizons

ROYAL SOCIETY OF CHEMISTRY

COMMUNICATION

View Article Online
View Journal | View Issue

Cite this: *Nanoscale Horiz.*, 2024, 9, 544

Received 27th November 2023,
Accepted 30th January 2024

DOI: 10.1039/d3nh00521f

rsc.li/nanoscale-horizons

Concurrent functional ultrasound imaging with graphene-based DC-coupled electrophysiology as a platform to study slow brain signals and cerebral blood flow under control and pathophysiological brain states†

Julie Meng Zhang, ‡[a] Eduard Masvidal-Codina,‡[bc] Diep Nguyen,[a] Xavi Illa,[cd] Julie Dégardin,[a] Ruben Goulet,[a] Elisabet Prats-Alfonso,[cd] Stratis Matsoukis,[ef] Christoph Guger,[e] Jose Antonio Garrido,‡[bg] Serge Picaud, ‡[a] Anton Guimerà-Brunet‡*[cd] and Rob C. Wykes ‡*[hi]

Current methodology used to investigate how shifts in brain states associated with regional cerebral blood volume (CBV) change in deep brain areas, are limited by either the spatiotemporal resolution of the CBV techniques, and/or compatibility with electrophysiological recordings; particularly in relation to spontaneous brain activity and the study of individual events. Additionally, infraslow brain signals (<0.1 Hz), including spreading depolarisations, DC-shifts and infraslow oscillations (ISO), are poorly captured by traditional AC-coupled electrographic recordings; yet these very slow brain signals can profoundly change CBV. To gain an improved understanding of how infraslow brain signals couple to CBV we present a new method for concurrent CBV with wide bandwidth electrophysiological mapping using simultaneous functional ultrasound imaging (fUS) and graphene-based field effect transistor (gFET) DC-coupled electrophysiological acquisitions. To validate the feasibility of this methodology visually-evoked neurovascular coupling (NVC) responses were examined. gFET recordings are not affected by concurrent fUS imaging, and epidural placement of gFET arrays within the imaging window did not deteriorate fUS signal quality. To examine directly the impact of infra-slow potential shifts on CBV, cortical spreading depolarisations (CSDs) were induced. A biphasic pattern of decreased, followed by increased CBV, propagating throughout the ipsilateral cortex, and a delayed decrease in deeper subcortical brain regions was observed. In a model of acute seizures, CBV oscillations were observed prior to seizure initiation. Individual seizures occurred on the rising phase of both infraslow brain signal and CBV oscillations. When seizures co-occurred with CSDs, CBV responses were larger in amplitude, with delayed CBV decreases in subcortical structures. Overall, our data demonstrate that gFETs are highly compatible with fUS and allow concurrent examination of wide bandwidth electrophysiology and CBV. This graphene-enabled technological advance has the potential to improve our understanding of how infraslow brain signals relate to CBV changes in control and pathological brain states.

New concepts

Neurovascular coupling (NVC) is a complex process that regulates regional cerebral blood volume (rCBV) to meet the dynamic energy needs of the brain, and involves the coordinated activity of neurons, astrocytes, and blood vessels. Imaging of rCBV, with traditional electrophysiology approaches are the current state-of-art methodology. However, this is only able to report two sides of a three-sided story. Metal-based electrodes are poorly suited to record infra-slow brain oscillations (ISO) and DC potential shifts, which likely influence both local field potential (LFP) recordings and rCBV; particularly in disease-relevant settings. Graphene micro-transistor (gFET) arrays overcome limitations of metal-based electrodes and can faithfully map DC-coupled electrographic responses and LFP with high fidelity. In this technical report, we demonstrate that flexible gFET arrays are compatible with functional ultrasound (fUS) and can be used to investigate how both fast and slow brain signals couple to blood flow under both physiological and pathophysiological conditions. The capability to obtain multi-modal measurements concurrently is particularly important for the study of individual and unpredictable brain events. Therefore, the proposed technique has the potential to revolutionize our understanding of how slow brain signals couple to regional blood flow during paroxysmal events, such as seizures and spreading depolarizations.

[a] *Sorbonne Université, INSERM, CNRS, Institute de la Vision, Paris F75012, France*
[b] *Catalan Institute of Nanoscience and Nanotechnology (ICN2), CSIC and BIST, Campus UAB, Bellaterra, Barcelona, Spain*
[c] *Centro de Investigación Biomédica en Red en Bioingeniería, Biomateriales y Nanomedicina (CIBER-BBN), Madrid, Spain. E-mail: anton.guimera@imb-cnm.csic.es*
[d] *Institute of Microelectronics of Barcelona, (IMB-CNM), CSIC, Spain*
[e] *G-Tec Medical Engineering GmbH, Austria*
[f] *Institute for Computational Perception, Johannes Kepler University, Linz, Austria*
[g] *ICREA, Barcelona, Spain*
[h] *University College London Queen Square Institute of Neurology, London, UK. E-mail: r.wykes@ucl.ac.uk*
[i] *Nanomedicine Lab, Division of Neuroscience, University of Manchester, UK*

† Electronic supplementary information (ESI) available. See DOI: https://doi.org/10.1039/d3nh00521f

‡ Authors contributed equally.

Introduction

Neurovascular coupling (NVC) is a complex process that ensures that the brain receives the blood flow it needs to function properly, involving the coordinated activity of neurons, astrocytes, and blood vessels. NVC is essential for normal brain function, and its dysfunction is linked to a number of neurological disorders.[1] Conventional methods to study NVC at the mesoscale, including subcortical brain regions, are limited by both the technology used to detect electrophysiological signals and the imaging approaches used to study blood flow. Electrophysiological methods typically acquire only AC-coupled signals with frequencies >0.1 Hz, due in part to the poor performance of traditional metal-based electrodes in recording slow brain potentials.[2,3] However, functional magnetic resonance imaging (fMRI) studies suggest that signals at 0.1 Hz and below, called infra-slow brain signals contribute to NVC.[4] fMRI itself is an indirect measure of blood flow based on changes in blood oxygenation, and uses strong magnetic fields complicating concurrent electrophysiological recordings. Therefore, to understand the contribution of infraslow brain signals, such as DC potential shifts and infraslow oscillations (ISO) to NVC, novel approaches combining cerebral blood volume (CBV) imaging with wide bandwidth DC-coupled electrophysiology are warranted. Graphene, a 2D material with exceptional electrical conductivity, is ideal for integration into neural interfaces.[5] Graphene field-effect transistor arrays (gFETs) demonstrate excellent recording stability and a high signal-to-noise ratio for DC-coupled measurements.[6] Flexible arrays of gFETs can be used to map fast and slow brain signals including seizures and spreading depolarisations with unsurpassed fidelity.[7,8] To investigate how both slow and fast electrographic signals couple to changes in CBV we used functional ultrasound (fUS): a method for identifying regions of brain activation by imaging transient changes in blood volume. fUS is based on backscattered echoes from red blood cells, allowing whole-brain imaging of NVC.[9] For preclinical studies, where imaging can be performed through a mouse skull, or *via* a craniotomy in larger species, fUS offers several advantages over fMRI including higher spatiotemporal resolution. It also permits imaging of deeper brain regions compared to other methods such as laser speckle contrast imaging.[9] In this study, we investigated the compatibility of surface DC-coupled electrophysiology recordings enabled by gFETs simultaneously with fUS imaging of CBV in anesthetized rats. Concurrent multi-modal recordings are important, particularly in relation to spontaneous, unpredictable events where inter-event variability will not permit the summation of unimodal acquired data. This approach permits recording both fast and infra-slow brain signals, which is important for understanding their relation in both normal and pathological brain states. We illustrate applications of this approach by measuring wide bandwidth electrical activity and CBV in response to visual stimulation, cortical spreading depolarisations, and seizures.

Results and discussion

To demonstrate the power of our experimental paradigm, we performed concurrent fUS imaging with graphene-based DC-coupled electrophysiology (fUS-gFET) in anesthetized rats subjected to physiological and pathological stimuli.

Compatibility of concurrent acquisition of CBV and DC-coupled electrophysiology during visual stimuli

The experimental design (Fig. 1a) consists of epidural placement of a thin ($\sim$10 μm-thick) polymeric device with embedded graphene microtransistors and the placement of a fUS probe above it using echography gel to ensure proper ultrasound transmission. The principles of fUS are presented in Fig. 1a (right box). An ultrasound tilted plane wave is generated from the transducer array within the probe and the recorded backscattered signals are used for reconstruction of compound fUS images, which upon coherent summation and clutter filtering, generate the final high resolution fUS image. The recording principle of a gFET is shown in the bottom box of Fig. 1a. Briefly, a bias voltage (V_{ds}) is applied across the graphene channel to promote current flow (I_{ds}) that fluctuates based on the signals at the graphene surface which is in contact with the neural tissue. Due to the excellent electrochemical stability of graphene and the FET-based acquisition mechanism, signals are acquired in DC-coupled mode with excellent signal fidelity.[6] Potential crosstalk effects between both modalities were examined. Activation of fUS acquisition (which uses 15 MHz ultrasound waves) did not affect the gFET signal quality. No detectable artifacts or changes in timeseries and LFP power were observed by switching fUS acquisition ON and OFF (Fig. 1b). Moreover, the presence of the gFETs embedded in a thin, flexible polyimide substrate did not result in imaging artefacts on fUS acquired images (Fig. 1c), further demonstrating the compatibility of these two distinct methodologies.

As a first demonstration of the technique's potential, we examined concurrent electrographic recordings and CBV changes during visual stimuli. Light stimulation (2 Hz, 50% duty cycle) to the contralateral eye induced ON/OFF potentials (Fig. 1f), and an increase in CBV in areas related to visual processing such as the superior colliculus (SC), lateral geniculate nucleus (LGN) and primary visual cortex (V1) (Fig. 1d and e, n = 3 animals) in accordance with literature,[10] validating the concurrent methodology.

Concurrent electrographic and blood volume responses to cortical spreading depolarisations

To demonstrate concurrent DC-coupled electrophysiology and CBV imaging, we performed acquisitions during induction of cortical spreading depolarisation (CSD). CSD is the most severe disruption of brain homeostasis that can occur in living neural tissue and is characterized by a sudden, near-complete collapse of the transmembrane ion gradients and a large-amplitude (tens of millivolts) negative shift in extracellular potential that lasts for tens of seconds.[11] We induced CSD by either mechanical manipulation (pinprick), or pharmacological (high extracellular potassium) administration *via* a small bur hole close to the imaging window (Fig. 2a) and mapped the propagation of the CSD across the cortex electrographically and haemodynamically simultaneously. Pinprick induced a cortical propagating wave of depolarisation (depolarisation duration 80 $\pm$ 33 s,

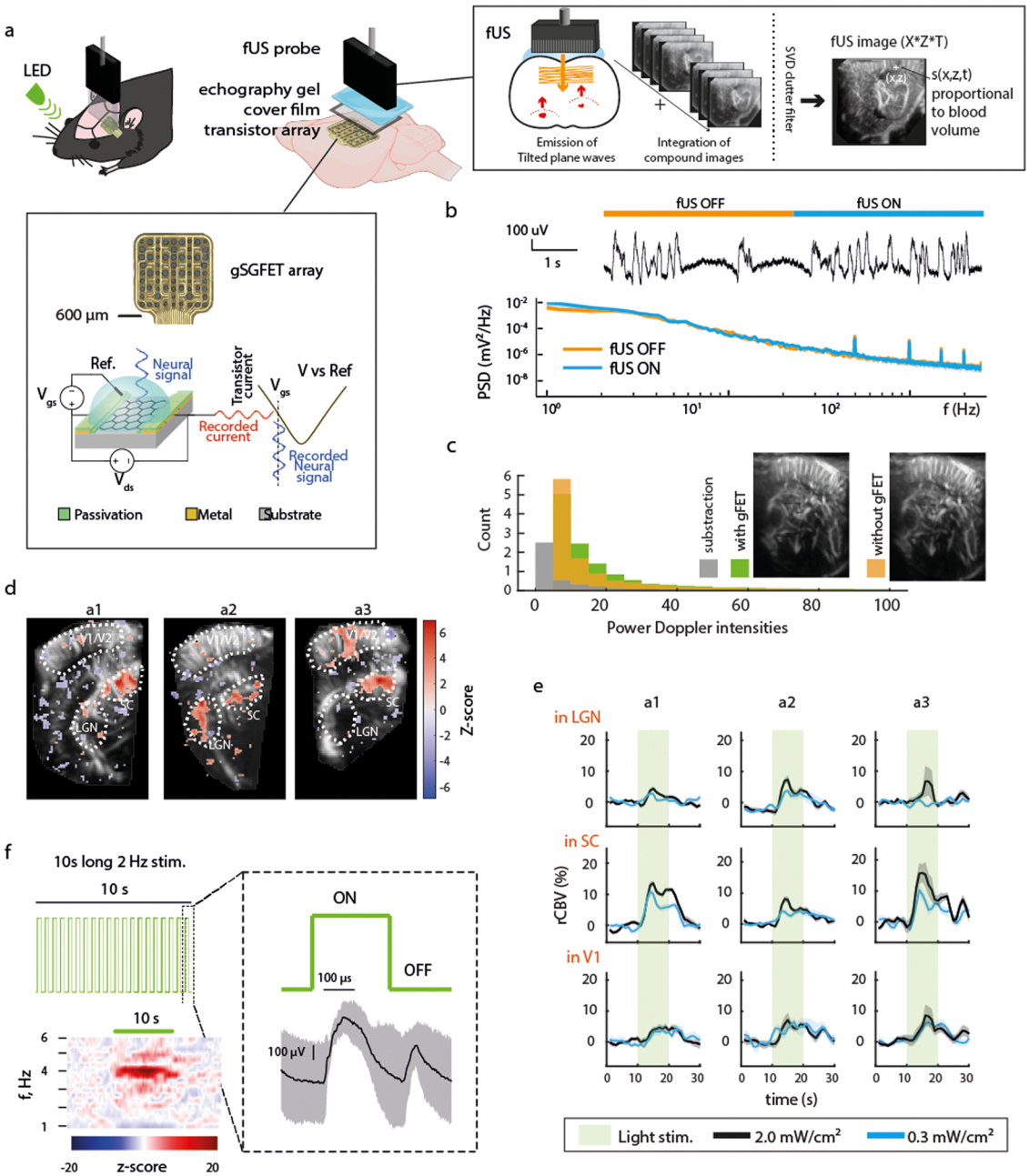

Fig. 1 Technological and functional compatibility of concurrent electrophysiological and functional ultrasound imaging. (a) Schematic of the experimental paradigm. An LED was used to visually stimulate the eye contralateral to electrographic and imaging recordings. Over the left hemisphere cortex of a rat, a large (3 × 9 mm) craniotomy was performed to be used as fUS imaging window (AP +1 to −8 mm, ML 0.5–3.5 mm). A 16 channel gSGFET array was positioned on the dura over visual/somatosensory cortex and the craniotomy sealed with a piece of cover film before application of transduction gel and placement of the fUS probe. Schematic cross-section of a graphene micro-transistor, with the driving voltage (V_{ds}) and the operation point selector voltage (V_{gs}) labelled. Current fluctuations in the drain-source current (I_{ds}) are then converted back to voltage using the transfer characteristics of the transistor ($I_{ds} = f(V_{gs})$ curve).[6] The principles of fUS imaging are shown in schematic form (right box). (b) Representative gFET-acquired raw electrophysiological signal and power spectrum density (PSD) during times when fUS-acquisition was switched ON or OFF. PSD line represents the median and shaded area the median absolute deviation of signals acquired with 13 gFETs for a single ON–OFF transition. (c) Representative fUS-acquired image with (green) or without (orange) gFET placement over the cortex underneath the fUS probe, histogram of pixel intensity, with or without array placement and subtraction (grey). (d) Z-score of correlation between stimulation pattern and rCBV for 3 different animals (a1, a2, a3). Region of interests ROIs are the visual cortex (V1), the superior colliculus (SC) and the lateral geniculate nucleus (LGN). (e) Averaged rCBV increase during the 10 s visual stimulation at the 3 selected regions. (f) Visual stimulation protocol consisted of 2 Hz light stimulus (50% duty cycle) during 10 s followed by 20 s without light stimulation repeated 10 times, *i.e.* total protocol duration of 5 min. Averaged z-scored power spectrogram during the 10 s light stimulation shows an increase in power at double of the LED stimulation frequency (4 Hz) as expected. Right: Median and median absolute deviation of the electrophysiological response recorded using a gFET in response to the visual stimulation. ON and OFF visually evoked potentials are observed.

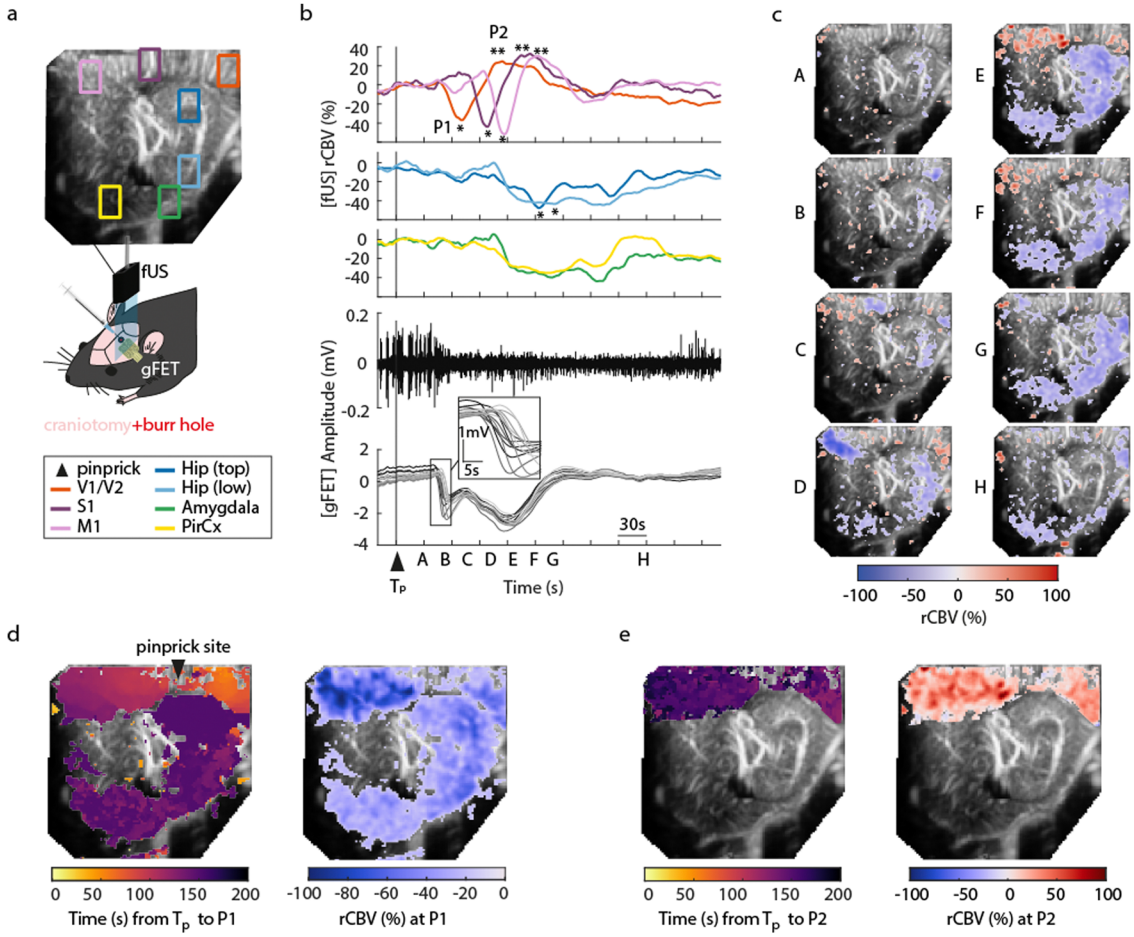

Fig. 2 Characterisation of cortical spreading depolarisations using simultaneous gFET epidural recordings and fUS. (a) Schematic of the experimental protocol. The fUS probe was placed on top of the array in sagittal orientation. Either pinprick or KCl stimulus was applied *via* a burr hole next to the craniotomy at bregma −7 mm. Above there is a fUS image with rectangles indicating different extracted regions of interest. The colour code for rCBV changes in different brain regions is shown below the schematic. (b)–(e) A CSD event occurring upon mechanical pinprick. (b) Time course of cerebral blood volume changes in visual areas (V1/V2, orange), somatosensory cortex (S1, brown), motor cortex (M1, pink), hippocampus (blue), and amygdala (green) and piriform cortex (yellow). Below: the electrographic response recorded using the graphene transistor array (gFET); local field potential signal from a single transistor (top, black trace), and DC signals from multiple transistors, with blow up to illustrate propagation (below, grey traces). T_p represents pinprick onset and P1 and P2 the first global minimum and global maximum of the rCBV response respectively. (c) Time course of CSD changes in rCBV through the sagittal plane of the brain. Letters correspond to the timepoints in (b). (d) (left) Propagation of P1 over time across the cortical and subcortical regions of the brain and (right) corresponding rCBV variations at P1. (e). Propagation of P2 over time across the cortical and subcortical regions of the brain (left) and corresponding rCBV at P2 (right).

9 CSDs from 5 rats), and a sustained period of cortical spreading local field potential depression (Fig. 2b). Recovery of neuronal activity assessed by local field potential power took approximately 7 minutes. The haemodynamic response to CSD in cortical regions was biphasic: an initial CBV decrease was subsequently followed by an increase. The peak decrease (P1) of CBV was of −53.32 ± 3.58%, starting in regions close to the site of induction (visual areas V1/V2), and slowly propagating to cortical regions further away from onset, first to the somatosensory cortex and then to the motor area (Fig. 2c and d). In all these cortical structures, the minimum peak was followed by a peak hyperaemia (P2) of 40.92 ± 13.21%, delayed by 47.17 ± 7.09 s from P1 (n = 9 pinprick CSDs from n = 5 animals) that also displayed propagation (Fig. 2e). CSD propagation speed calculated from CBV changes was calculated at 6.05 ± 1.28 mm min^{-1}, comparable to previously reported values.[12] Similar results were obtained when CSD was induced *via* localised administration of potassium chloride to the burr hole. CSD duration 46 ± 34 s, propagation speed 5.2 ± 1.57 mm min^{-1}, P1 (rCBV −31.90 ± 1.74%), P2 (rCBV 45.34 ± 8.66%), (5 CSDs from 4 rats). Correlations (at the site of the array) between the DC signal and CBV were observed. The DC depolarisation onset correlated with the P1 CBV decrease peak while the P2 hyperaemia recovery correlated with the depolarisation recovery. Interestingly we observed delayed subcortical blood flow changes indicating that neurovascular responses to a CSD are not restricted to the cortex. Although the haemodynamic response to CSD in the cortex has been well studied and reported, the technical approaches taken usually only detect superficial blood flow changes, resulting in an assumption that changes in blood flow are limited to the cortex. Recent fUS

imaging studies reported that CSD can induce complex subcortical CBV changes.[13,14] Our data reveal delayed CBV decreases in subcortical regions including the hippocampus, amygdala and piriform cortex (Fig. 2b–d). However, functional hyperaemia was confined to cortical regions (Fig. 2e). The mechanisms underlaying such observations remain to be elucidated. The combination of larger area DC-coupled surface arrays, or penetrating probes,[8] with fUS imaging will permit more advanced studies into the global impact of CSD to brain function.

Blood volume response to seizures and seizure-associated spreading depolarisations

Seizures can be generated by a coupled dynamical system in which there are both fast and slow processes[15] and induce large haemodynamic responses. Pre-seizure DC potential shifts and ISOs may favor the transition to seizure by opening seizure susceptibility windows,[8] but the role of blood flow in the transition to seizure is poorly understood. It has been reported that preictal blood flow changes can occur several seconds before seizure onset.[16–18] To investigate the temporal relationship between CBV changes, ISOs and seizure onset, we induced acute seizures by focal administration of a chemoconvulsant (4-AP) to the visual cortex. Recurrent seizures typically arise several minutes after injection and are detected by the epidurally placed gFET array (Fig. 3a). We observed oscillations in cortical rCBV which preceded the seizure onset by 187 ± 29 s (n = 4 animals) (Fig. 3b). These oscillations grew in amplitude until the onset of seizures. There was one cycle per seizure. The minimum of the rCBV oscillation (91 ± 9%) occurred 5 ± 3 s before seizure onset while the crest of the oscillation had peak

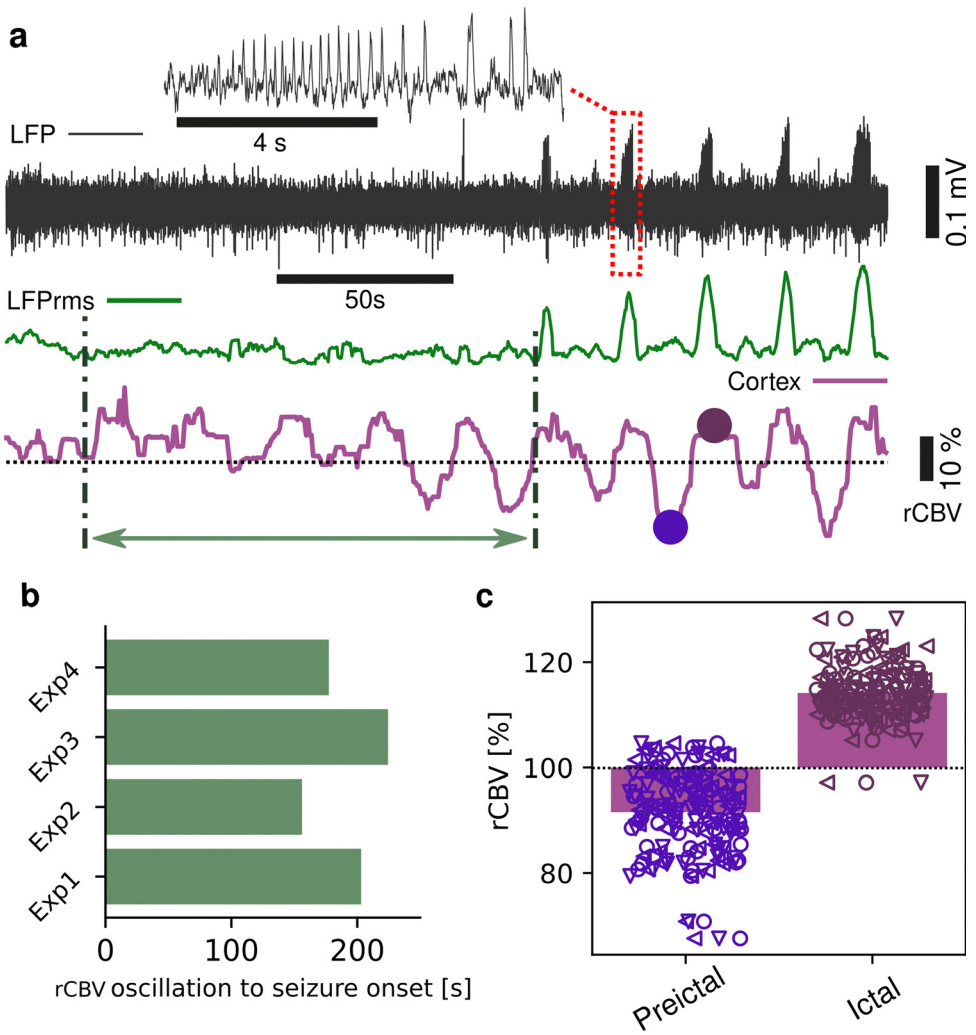

Fig. 3 Blood flow changes precede the onset of chemoconvulsant-induced seizures. (a) Representative high-pass filtered (>1 Hz) recording (black trace), with corresponding root mean square signal (rms, green trace) from a single transistor for the period post-injection of chemoconvulsant (4-AP) until the onset of seizures. Red box highlights a seizure event, as shown in the blow up above. Concurrent cortical rCBV imaging (purple trace) is shown below, where oscillations can be observed. Green arrow depicts the time between start of the rCBV oscillations and the first electrographically detectable seizure. Dots indicate the minimum and maximum of the rCBV oscillations in one representative period. (b) Bar plot of the time between rCBV oscillation start and seizure onset, n = 4 animals. (c) Bar and scatter plot of the change in rCBV during preictal and ictal states as defined by the electrographic onset of seizure, n = 92 seizures from 3 animals. Marker shape refers to individual animals.

rCBV (114 ± 4%) and occurred during the ictal discharge (Fig. 3a and c). DC-coupled electrophysiology revealed an ISO, also with one cycle per seizure (Fig. 4a and b). Although the time course of the ISO and rCBV cycles were similar, there was heterogeneity in the order of events, with the phase of the ISO sometimes fractionally preceding rCBV and in other instances CBV occurring prior to ISO (Fig. 4e). On average ISO and rCBV rises occurred −7.6 ± 3.1 seconds and −5.3 ± 3.4 s respectively before the onset of seizure. We attribute the heterogeneity in ISO and rCBV order between seizures and animals partially to the relatively small gFET arrays used in this study (1.6 mm × 1.6 mm). We have previously reported that the onset of 'active' DC shifts are spatially restricted[8] and therefore we hypothesize that it is possible that some seizures arise directly underneath the array, whereas others may start further away which could explain the slight variability in ISO/CBV order. Future studies employing larger gFET arrays will be necessary to gain further insight into the temporal order of ISO/CBV signals. Our results demonstrate a tight correlation, with phase-amplitude coupling between ISO's and LFP in addition to rCBV (Fig. 4c and d), suggesting that the generator(s) for seizure-associated ISOs and rCBV oscillations may share a common mechanism. Due to their ability to generate slow, seizure-related DC shifts[19] and their role in mediating NVC responses[20] astroglia cells may contribute significantly to the observed responses and deserve further investigation. In this regard, our technological approach might allow future dissection of pathways which result in this form of activity and provide insight into seizure genesis with important therapeutic implications particularly for spontaneous seizures.

Seizures have been reported to co-occur with spreading depolarisations,[8,21] but due to the prominence of AC-coupled electrophysiology used by the epilepsy community

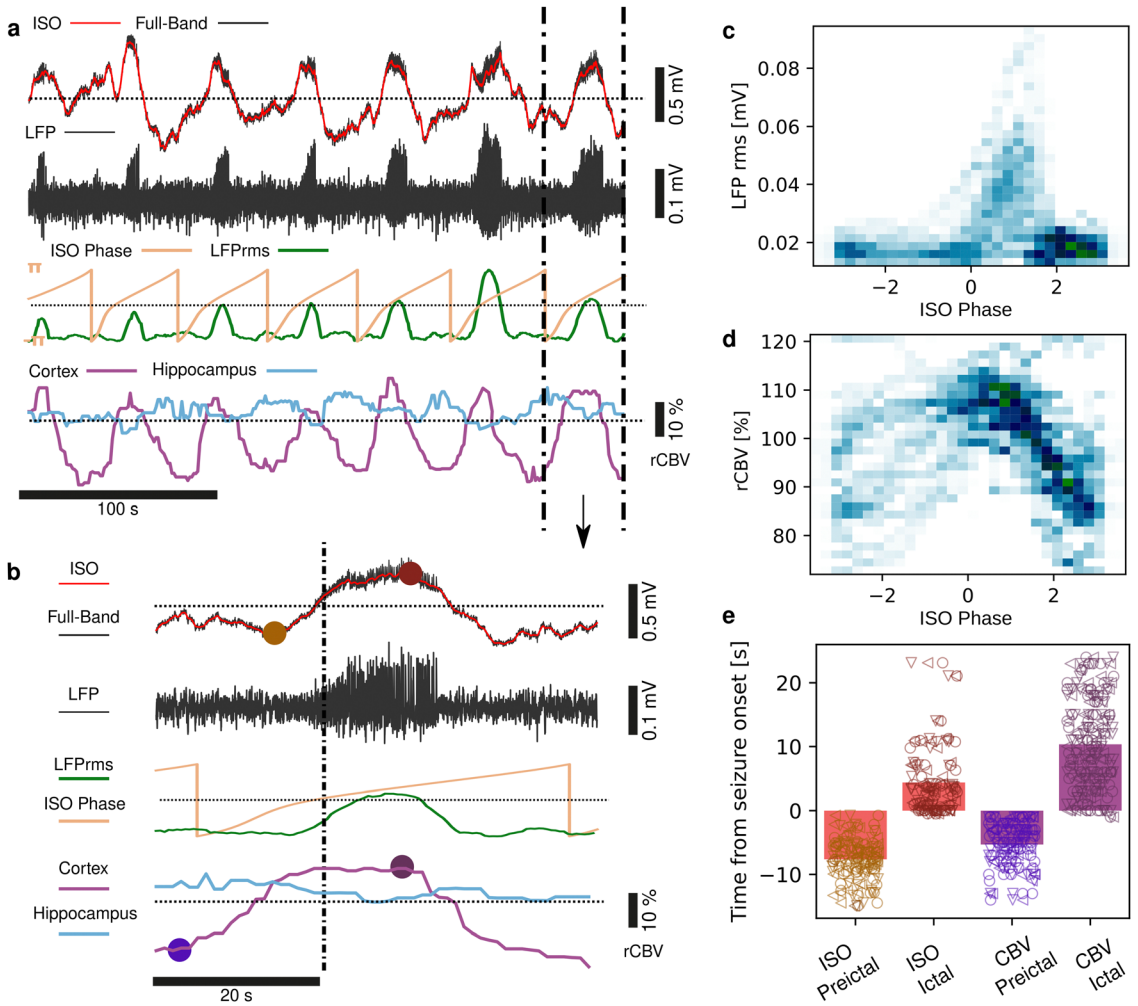

Fig. 4 Correlations between rCBV, ISO and seizures. (a) Raw DC-coupled recording of 7 seizures (black), with the DC potential (<1 Hz) displayed in red. The signal filtered above 1 Hz is shown below (black), with the LFP rms displayed in green, and the ISO phase (0.02–0.25 Hz) in yellow. rCBV from a region of interest in the cortex (purple) and hippocampus (blue) are shown at the bottom. (b) Blow up of a single seizure event illustrating the amplitude-phase correlation between ISO, seizure and cortical rCBV. The brown and purple dots mark the trough and peaks of the ISO and rCBV respectively. (c) Density distribution of the ISO phase and seizure LFP rms. (d) Density distributions of the ISO phase and rCBV. (e) Time of ISO and CBV increase prior to seizure onset and peak time during the ictal state. The rise of the ISO and CBV occurred prior to seizure onset, peaking towards the end of ictus, before dropping again. n = 92 seizures from 3 animals. Marker shape refers to individual animals.

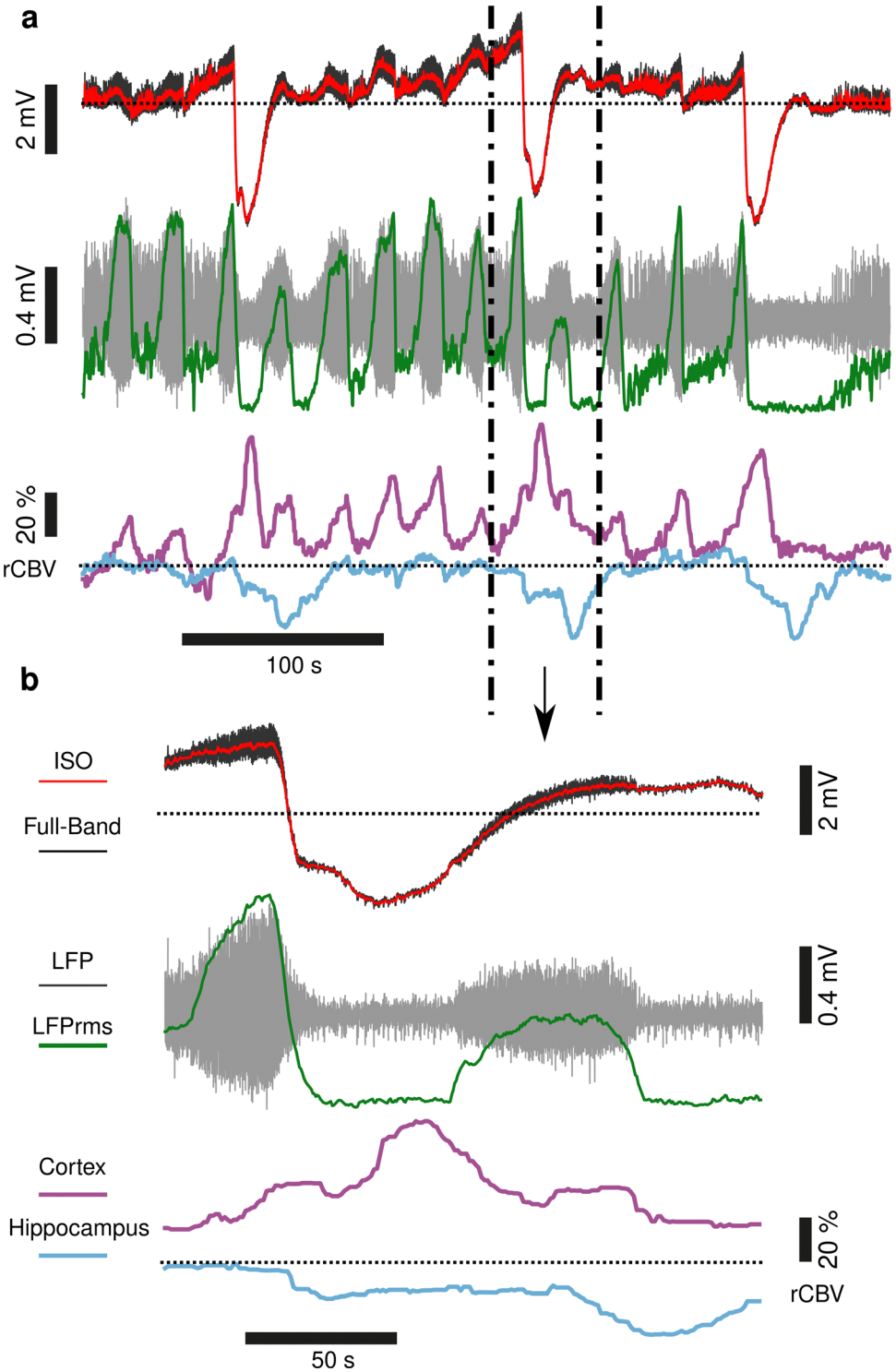

Fig. 5 Seizures associated with spreading depolarisation result in hyperaemia in cortical regions and decreased blood flow in subcortical regions. (a) DC-coupled recording (black) of multiple seizures and 3 CSDs, with the DC potential (<1 Hz) displayed in red. The signal filtered above 1 Hz is shown below (grey), with the LFP rms displayed in green. rCBV from a region of interest in the cortex (purple) and hippocampus (blue) are shown below. (b) Blow up of an individual seizure and associated spreading depolarisation event. In response to the seizure and SD there is a large increase in rCBV in the cortex, with a delayed decrease in rCBV in the hippocampus; N = 3 seizure-SD events, N = 1 animal.

this is a largely overlooked phenomenon even though it has important clinical implications.[22,23] When seizures were associated with CSD, we observed larger and more sustained increases in rCBV post-seizure in cortical regions and delayed and prolonged decreased rCBV in subcortical regions including the hippocampus (Fig. 5). In summary, using a model of

chemoconvulsant-induced seizures we report pre-seizure rCBV oscillations and coupling between infra-slow brain signals and blood flow at seizure onset. Consistent with other recent findings, we observed a decrease in blood flow to the brain in the seconds before transition to seizure, and an increase during the seizure.[24,25] Seizures that occurred with CSDs showed more complex NVC responses, with increases of rCBV in cortical regions and a delayed reduction of rCBV in subcortical regions including the hippocampus.

Conclusions

Novel approaches combining wide bandwidth DC-coupled electrophysiology with electrophysiology compatible methods for deep imaging of cerebral blood volume are warranted for deciphering the relation between electrical and haemodynamic changes during physiological and pathophysiological brain states. Here, we validate the instrumental and functional compatibility of gFETs and fUS modalities, enabling the study of how fast and infra-slow electrical brain signals relate to haemodynamic changes. Our results show that seizures can be preceded by detectable changes in the brain, including blood flow, and neuronal and/or astroglial activity. These changes likely reflect a shift in excitability towards a state that is more liable to produce a seizure. This has important implications, not only for our mechanistic understanding of the transition to seizure, but also in identifying novel targets that could prevent seizure onset. Additionally, as the infraslow and CBV changes occur seconds to minutes before seizure onset, these measurements could be incorporated into seizure warning algorithms or used to trigger closed-loop neuromodulation with the aim of preventing seizure occurrence. The technological platform introduced in this study based on concurrent fUS imaging with DC-coupled electrophysiology enabled by graphene microtransistor arrays provides an ideal experimental set up for exploring these fundamental questions. Indeed, this approach is not limited to epilepsy research. A number of diseases are associated with spreading depolarisations, ISO, and altered blood flow; including stroke, traumatic brain injury, migraine with aura and glioblastoma. Anesthesia is a limitation of this study; as it modulates neural activity, baseline CBV and the frequency of spreading depolarisations.[26] Future studies in awake brain employing 3D fUS imaging, with both large-coverage epidural and penetrating gFETs, will provide unparalleled insight into the bidirectional relationship between electrographic and haemodynamic changes in both health and disease.

Experimental section

NVC was examined under three experimental approaches: visual stimulation *via* full-field LED illumination of the contralateral eye; induction of CSD by either mechanical (pinprick), or chemical (high potassium 1 μl of 100 mM injected into the superficial cortex) approaches; and initiation of seizures *via* injection of 1 μl of 50 mM 4-aminopyridine (4-AP) to the visual cortex. For each stimulus, epidural DC-coupled electrographic signals from the visual/somatosensory cortex of a single hemisphere were recorded using polyimide-based flexible graphene field-effect microtransistor arrays. These are 1.6 × 1.6 mm in size, with a 4 × 4 arrangement of 50 × 50 or 100 × 100 μm^2 channel sizes. The fabrication was performed at the clean-room of the Institut de Microelectrònica de Barcelona (IMB-CNM, CSIC) following the process described in previous studies.[6,7] Concurrent to the electrographic recordings, functional ultrasound imaging (fUS) of the brain was used to explore neural activation in the cortex and deeper subcortical structures.

Animal experiments and surgical details

A total of 14 Long Evans (LE) wild-type rats were used for this study. Rats were co-housed in ventilated cages with food and water ad libidum with enrichment. The temperature in the animal facility was maintained at 22 ± 2 °C and light cycle was reversed every 12 hours. All animal experiments were completed in accordance with the Charles Darwin No. 5 Ethics Committee in Animal Experimentation in the approved animal facilities associated to the Vision Institute (registration number APAFIS#24563-2020030614031084 v6). Half an hour before the surgical intervention, the rats were injected subcutaneously with Buprenorphine (0.05 mg kg^{-1}, Buprecare®, Axience, France) and Dexamethasone (0.7 mg kg^{-1}, Dexazone®, Virbac, France) to reduce any pain and inflammation. After being shaved, a local analgesic, Lidocaine (4 mg kg^{-1}, Laocaïne®, MSD, France) was administered subcutaneously under the scalp skin and Xylocaine gel (2%) was applied in the ears. Anaesthesia was provided by 5% gaseous induction of isoflurane (Isorane®, Axience, France) and maintained at 2–3%. Animals were placed in a stereotaxic frame. The body temperature was maintained at 37 °C with a heating plate. Drops of ocular gel (Lubrithal®, Dechra, France) were delivered on the eyes of the rats to avoid drying out and were then covered with a black cloth for dark adaptation. The skin was disinfected with iodopovidone solution (Vetedine®, Vetoquinol, France) and incised. Remaining skin parts were removed, and the skull was cleaned with oxygenated water. A unilateral craniotomy was performed to expose the dura from motor to visual cortical regions (left hemisphere). A burr hole was drilled next to the cranial window in the same brain hemisphere, at Bregma −7 mm (visual cortex), to enable access to the brain for CSD induction (pinprick or KCl) and injection of chemoconvulsant in the cortex for initiation of epileptiform and seizure activity. The array was placed over the visual/somatosensory cortical area. A piece of plastic (TPX® polymethylpentene, GoodFellow Cambridge, UK) was cut to fit the craniotomy and placed on top of the array. The fUS probe was placed on top of this, after applying generous drops of ultrasound gel. The probe was positioned coronally at bregma −5.5 mm for light stimulation experiments, and between midline (ML) +3.75 and 4.3 mm sagittally for other stimuli. A reference electrode, a chloride-coated silver wire, was placed in the contralateral neck muscle. The animals were kept under isoflurane anaesthesia for up to 4 hours and euthanized at the end of the experiment by

intracardiac injection overdose of euthanasian (200 mg kg^{-1}, Exagon®, Axience, France).

Light stimulation

Light stimulation was performed with a white full-field LED (MWWHLP1, ThorLabs, USA) controlled by a stimulus generator (STG 4002, Multi-Channel Systems, Germany) was used on 3 LE rats. The protocol consisted of 2 Hz light stimulus (50% duty cycle) during 10 s followed by 20 s without light stimulation repeated for 10 times, *i.e.*, a total protocol duration of 5 min. The LED amplitude was set at high intensity (2.0 mW cm^{-2}) or low intensity (0.3 mW cm^{-2}) in compliance with animal safety rules.

Induction of CSDs and seizures

CSDs were induced by either pricking the surface of the brain with a needle (31G), n = 5 animals, or injection of a high potassium solution directly into the superficial cortex *via* the pre-drilled bur hole (1 µl of 100 mM, n = 4 animals). To elicit seizures 0.5–1 µl of 50 mM 4-aminopyridine (4-AP) was injected through the bur hole close to the edge of the gFET array (n = 4 animals).

gFET calibration and analysis

Signal acquisition. Electrophysiological recordings were performed using flexible gFETs arrays. The transistor arrays were carefully connected to a PCB and lowered onto the dural surface. Whereas most currently available electrodes are passive, gSGFETs are active devices that transduce local voltage changes to current and permit a wide recording bandwidth.[6] The *in vivo* recordings were conducted using a custom g.HIamp biosignal amplifier (g.RAPHENE, g.tec medical engineering GmbH Austria). This system provides precise control over V_s and V_d bias voltages and current-to-voltage conversion for up to 16 gFET channels. The system splits the 16 input signals into two distinct frequency bands, each with different amplification characteristics. One is a low-pass filtered (LPF) DC band, featuring a cutoff frequency set at 0.16 Hz and a gain of 10^4. The second one is an AC bandpass filtered (BPF) band, covering a frequency range from 0.16 Hz to 6 kHz and a gain of 10^6. This setup is designed to prevent amplifier saturation. The signal resolution is 24 bits and the chosen sampling frequency has been set to 9.6 kHz. On the software side, the interface is managed through two separate Simulink models. The first model conducts a V_{gs} voltage sweep to acquire the $I_{ds} = f(V_{gs})$ curve for each microtransistor. This process aids in assessing the gFETs performance and determining the optimal bias point. The optimal bias point is calculated as the voltage at which the average across the arrays of the absolute transconductance is maximum. Example transfer curves from three experiments are shown in Fig. S1 (ESI†) illustrating the high homogeneity in optimal bias current across individual transistors on an array. The second model serves the purpose of recording and storing electrophysiology signals, as well as setting the appropriate V_s and V_d voltages.

Data calibration. All electrophysiological data were calibrated using Python 3.9 packages (Matplotlib, Numpy, Neo) and the custom library PhyREC (**https://github.com/aguimera/PhyREC**). The conversion of the recorded current signals (LPF and BPF) to a voltage signal was performed by summation of the two signals and inverse interpolation in the *in vivo*/chronic measured transfer curve of the corresponding gSGFET. The transfer curves were always measured at the beginning and end of every recording to ensure that no significant variations were present and to detect any malfunctioning transistor.

Data analysis. All electrophysiological data were analysed using Python 3.9 packages (Matplotlib 3.2.0, Numpy 1.17.4, Pandas 0.25.3, Seaborn 0.9.0, Scipy 1.11.1 and Neo 0.8.0) and the custom library PhyREC (**https://github.com/aguimera/PhyREC**). CSD analysis methods have previously been reported.[7] No high pass filtering is applied to the recorded extracellular potentials for the analysis of CSD waveforms, extraction of CSD parameters or plotting to avoid any signal distortion. Briefly, for each CSD extracellular voltage shift the duration was extracted. Raw signals were down-sampled to 3 Hz and zero voltage was set to the average value of the 5 s before the light stimulus. We defined the onset of the CSD as the onset of the negative shift with a threshold at −1 or −2 mV. CSD duration was defined as the time that the extracellular voltage remained below threshold. For analysis of seizure and CBV dynamics, the onset time of seizures was determined by defining a threshold of 0.025 mVrms on the signal power of LFP band (1 Hz to 50 Hz), then the time of max and min value for CBV and ISO signals was extracted for each seizure relative to its onset time. ISO phase was calculated by Hilbert transform after applying a narrow band pass filter (0.02 Hz 0.025 Hz) with a frequency range selected according with the periodicity of seizures.

fUS acquisition and analysis

The fUS probe is composed of a linear ultrasound probe (128 piezoelectric elements, 15 MHz, 110 µm pitch and 8 mm elevation focus, Vermon, France), connected to an ultrafast ultrasound scanner (Aixplorer, Verasonics, France) controlled through Matlab. Detailed physics principles behind fUS can be found in previous literature,[9,27] and are illustrated in Fig. 1a. Briefly, a sequence of tilted plane waves (11, angles from −10° to +10° with a 2° step) are simultaneously emitted by the transducers and their backscattered echoes are recorded. To obtain a high-resolution image, the sequence is repeated 200 times at 500 Hz which takes 0.4 s in total per image. Beamforming of the echoed signal enables reconstruction of the imaged brain slice and takes less than 0.6 s. The final image sampling rate is 1 Hz, resulting in a compound image (IQ) created per second. After acquisition, the compound images are filtered (details below) to remove background noise and the resulting power Doppler signals (proportional to the cerebral blood volume (CBV)) are obtained. Pre-processing of acquired images consisted of using singular value decomposition (SVD) with a clutter filter at λ = 60 to filter out singular values linked to the tissue space.[28] The power Doppler signals retrieved (PwD) is proportional to blood volume. The signals PwD were

then smoothed (Gaussian 3 × 3 filter) and analysed offline using Matlab. Baseline signal (BL) was calculated by averaging PwD during the first 30 s of acquisitions for light stimulation experiments and during the time before pinprick for other stimuli. The cerebral blood flow (CBV) was normalised into a relative steady-state value (rCBV) and calculated as the following:

$$\mathrm{rCBV} = \frac{(\mathrm{PwD} - \mathrm{BL})}{\mathrm{BL}} \times 100(\%)$$

Images were manually registered.

Light stimulation experiments

Correlation heatmaps between stimulation pattern and Doppler data were calculated using a global linear model[29] with Benjamini correction ($q < 0.1$). Lateral geniculate nucleus (LGN), superior colliculus (SC) and visual cortex (V1/V2) ROIs were identified according to the Paxinos & Watson rat brain atlas.[30] In these ROIs, rCBV was averaged over successive repetitions.

Pinprick, KCl and 4-AP injection experiments

Rectangle ROIs (15 × 10 voxels) were selected in the visual cortex (V1), somatosensory cortex (S1), and other subcortical regions such as Hippocampus (Hip), Thalamus (Thal) or Amygdala (Amygd). For pinprick and KCl experiments, global minimum (P1) and global maximum (P2) peaks were identified on rCBV plots during the CSD events (n = 9 events for 5 animals). Peak rCBV percentage and time from onset stimulus were quantified across subjects. CSD propagation heatmaps were represented for P1, P2 in terms of rCBV amplitude and time from stimulus onset. Voxels for which rCBV amplitude at P1 was below three times the baseline standard deviation were discarded. Additionally, for voxels in cortical regions, the time at which P1 occurs from onset time *versus* distance of the voxels from onset point was calculated. CSD speed (mm min^{-1}) was obtained by calculating the slope of the linear fit to this plot.

Author contributions

Conceptualization: S. P., A. G.-B., R. W.; investigation: D. N., J. Z., E. M.-C., A. G.-B., R. W.; resources: J. D., R. G., X. I., E. P. A., J. A. G., S. M., C. G.; visualization and writing: J. Z., E. M.-C., A. G.-B., R. W.

Conflicts of interest

SM & CG work for g-tec medical engineering, GmbH Austria. A.G. and J.A.G. would like to declare that they hold interest in INBRAIN Neuroelectronics that has licensed the gFET technology described in this manuscript. All other authors have no competing interests.

Acknowledgements

This research was funded by the European Union's Horizon 2020 research and innovation programme under grant agreement no. 881603 (Graphene flagship Core 3). This project has also received funding from the European Union's Horizon 2020 research and innovation programme under the Marie Skłodowska-Curie grant agreement no. 861423 (enTRAIN Vision). We acknowledge the LabEx LIFESENSES (ANR-10-LABX-65) and IHU FOReSIGHT (ANR-18-IAHU-01). RW holds a Senior Research Fellowship funded by the Worshipful Company of Pewterers. ICN2 is supported by the Severo Ochoa Centres of Excellence programme (Grant CEX2021-001214-S), funded by MCIN/AEI/10.13039.501100011033, and by the CERCA Programme of Generalitat de Catalunya. E. M. C. acknowledges grant FJC2021-046601-I funded by Agencia Estatal de Investigación of Spain and the European Union NextGenerationEU/PRTR. This work has made use of the Spanish ICTS Network MICRONANOFABS, partially supported by MICINN and the ICTS NANBIOSIS, specifically by the Micro-NanoTechnology Unit U8 of the CIBER-BBN. This research has been also supported by funding from the Generalitat de Catalunya (2021SGR00495), MCIN/AEI/10.13039/501100011033 and "ERDF A way of making Europe" (grant PID2021-126117NA-I00), and the "European Union NextGenerationEU/PRTR", (grant PLEC2022-009232), and CIBER-Consorcio Centro de Investigación Biomédica en Red-(CB06/01/0049), Instituto de Salud Carlos III, Ministerio de Ciencia e Innovación.

References

1 T. L. Stackhouse and A. Mishra, *Front. Cell Dev. Biol.*, 2021, **9**, 702832.
2 C. Li, R. K. Narayan, P. M. Wu, N. Rajan, Z. Wu, N. Mehan, E. V. Golanov, C. H. Ahn and J. A. Hartings, *J. Neural Eng.*, 2016, **13**, 016008.
3 J. A. Hartings, *Nat. Mater.*, 2019, **18**, 194–196.
4 P. J. Drew, C. Mateo, K. L. Turner, X. Yu and D. Kleinfeld, *Neuron*, 2020, **107**, 782–804.
5 K. Kostarelos, M. Vincent, C. Hebert and J. A. Garrido, *Adv. Mater.*, 2017, **29**, 1700909.
6 E. Masvidal-Codina, X. Illa, M. Dasilva, A. B. Calia, T. Dragojevic, E. E. Vidal-Rosas, E. Prats-Alfonso, J. Martinez-Aguilar, J. M. De la Cruz, R. Garcia-Cortadella, P. Godignon, G. Rius, A. Camassa, E. Del Corro, J. Bousquet, C. Hebert, T. Durduran, R. Villa, M. V. Sanchez-Vives, J. A. Garrido and A. Guimera-Brunet, *Nat. Mater.*, 2019, **18**, 280–288.
7 E. Masvidal-Codina, T. M. Smith, D. Rathore, Y. Gao, X. Illa, E. Prats-Alfonso, E. D. Corro, A. B. Calia, G. Rius, I. Martin-Fernandez, C. Guger, P. Reitner, R. Villa, J. A. Garrido, A. Guimerà-Brunet and R. C. Wykes, *J. Neural Eng.*, 2021, **18**(5), 055002.
8 A. Bonaccini Calia, E. Masvidal-Codina, T. M. Smith, N. Schäfer, D. Rathore, E. Rodríguez-Lucas, X. Illa, J. M. De la Cruz, E. Del Corro, E. Prats-Alfonso, D. Viana, J. Bousquet, C. Hébert, J. Martínez-Aguilar, J. R. Sperling, M. Drummond, A. Halder, A. Dodd, K. Barr, S. Savage, J. Fornell, J. Sort, C. Guger, R. Villa, K. Kostarelos, R. C. Wykes, A. Guimerà-Brunet and J. A. Garrido, *Nat. Nanotechnol.*, 2022, **17**, 301–309.

9 E. Macé, G. Montaldo, I. Cohen, M. Baulac, M. Fink and M. Tanter, *Nat. Methods*, 2011, **8**, 662–664.
10 M. Gesnik, K. Blaize, T. Deffieux, J. L. Gennisson, J. A. Sahel, M. Fink, S. Picaud and M. Tanter, *NeuroImage*, 2017, **149**, 267–274.
11 J. P. Dreier, *Nat. Med.*, 2011, **17**, 439–447.
12 D. Pietrobon and M. A. Moskowitz, *Nat. Rev. Neurosci.*, 2014, **15**, 379–393.
13 L. Bourgeais-Rambur, L. Beynac, J.-C. Mariani, M. Tanter, T. Deffieux, Z. Lenkei and L. Villanueva, *J. Neurosci.*, 2022, **42**, 6295–6308.
14 C. Rabut, M. Correia, V. Finel, S. Pezet, M. Pernot, T. Deffieux and M. Tanter, *Nat. Methods*, 2019, **16**, 994–997.
15 V. K. Jirsa, W. C. Stacey, P. P. Quilichini, A. I. Ivanov and C. Bernard, *Brain*, 2014, **137**, 2210–2230.
16 U. J. Chaudhary, D. W. Carmichael, R. Rodionov, R. C. Thornton, P. Bartlett, S. Vulliemoz, C. Micallef, A. W. McEvoy, B. Diehl, M. C. Walker, J. S. Duncan and L. Lemieux, *Brain*, 2012, **135**, 3645–3663.
17 M. N. DeSalvo, U. Schridde, A. M. Mishra, J. E. Motelow, M. J. Purcaro, N. Danielson, X. Bai, F. Hyder and H. Blumenfeld, *NeuroImage*, 2010, **50**, 902–909.
18 C. Tangwiriyasakul, S. Perani, M. Centeno, S. N. Yaakub, E. Abela, D. W. Carmichael and M. P. Richardson, *Brain*, 2018, **141**, 2981–2994.
19 H. Caspers, E. J. Speckmann and A. Lehmenkühler, *Rev. Physiol., Biochem. Pharmacol.*, 1987, **106**, 127–178.
20 A. Lia, A. Di Spiezio, M. Speggiorin and M. Zonta, *Front. Netw. Physiol.*, 2023, **3**, 1162757.
21 I. Aiba, Y. Ning and J. L. Noebels, *JCI Insight*, 2023, **8**(15), e170399.
22 I. C. M. Loonen, N. A. Jansen, S. M. Cain, M. Schenke, R. A. Voskuyl, A. C. Yung, B. Bohnet, P. Kozlowski, R. D. Thijs, M. D. Ferrari, T. P. Snutch, A. van den Maagdenberg and E. A. Tolner, *Brain*, 2019, **142**, 412–425.
23 I. Aiba and J. L. Noebels, *Sci. Transl. Med.*, 2015, **7**(282), 282ra46.
24 M. Nourhashemi, M. Mahmoudzadeh, C. Heberle and F. Wallois, *Neurophotonics*, 2023, **10**, 025005.
25 H. K. Lim, N. You, S. Bae, B. M. Kang, Y. M. Shon, S. G. Kim and M. Suh, *J. Cereb. Blood Flow Metab.*, 2021, **41**, 1145–1161.
26 I. E. Mosneag, S. M. Flaherty, R. C. Wykes and S. M. Allan, *Neuroscience*, 2023, DOI: **10.1016/j.neuroscience.2023.11.034**.
27 M. Tanter and M. Fink, *IEEE Trans. Ultrason. Ferroelectr. Freq. Control.*, 2014, **61**, 102–119.
28 C. Demené, T. Deffieux, M. Pernot, B. F. Osmanski, V. Biran, J. L. Gennisson, L. A. Sieu, A. Bergel, S. Franqui, J. M. Correas, I. Cohen, O. Baud and M. Tanter, *IEEE Trans. Med. Imaging*, 2015, **34**, 2271–2285.
29 K. J. Friston, in *Neuroscience Databases: A Practical Guide*, ed. R. Kötter, Springer US, Boston, MA, 2003, pp. 237–250, DOI: **10.1007/978-1-4615-1079-6_16**.
30 G. Paxinos and C. Watson, *The rat brain in stereotaxic coordinates*, Elsevier, Academic Press, Compact 7th edn, 2018.

